Pulse front tilt control using non-collimated beams in a single pass grating compressor

Article *in* Optics Express · February 2020

DOI: 10.1364/OE.28.007678

CITATIONS
5

READS
189

7 authors, including:

Gonçalo Figueira
University of Lisbon
88 PUBLICATIONS **491** CITATIONS
SEE PROFILE

Luis Carlos da Silva Braga
SANTA TERE
8 PUBLICATIONS **49** CITATIONS
SEE PROFILE

Sajidah Ahmed
University of Bath
2 PUBLICATIONS **15** CITATIONS
SEE PROFILE

Marco Galimberti
Science and Technology Facilities Council
181 PUBLICATIONS **3,270** CITATIONS
SEE PROFILE

Research Article | Vol. 28, No. 5 / 2 March 2020 / Optics Express 7678
Optics EXPRESS

Pulse front tilt control using non-collimated beams in a single pass grating compressor

GONÇALO FIGUEIRA,[1,*] LUÍS BRAGA,[1] SAJIDAH AHMED,[2] ALEXIS BOYLE,[2] MARCO GALIMBERTI,[2] MARIO GALLETTI,[1,2] AND PEDRO OLIVEIRA[2]

[1]GoLP, Instituto de Plasmas e Fusão Nuclear, Instituto Superior Técnico, University of Lisbon, 1049-001 Lisbon, Portugal
[2]Central Laser Facility, Science and Technology Facilities Council Rutherford Appleton Laboratory, Harwell Science and Innovation Campus, Didcot OX11 0QX, UK
*goncalo.figueira@tecnico.ulisboa.pt

Abstract: High power laser systems based on the chirped pulse amplification (CPA) technique make use of grating pairs to compress the pulse to a short duration. When designing the pulse compressor, it is normally assumed that good beam collimation is a strong requirement in order to avoid spatio-temporal couplings. We analyze the propagation through a single pass compressor without the good collimation approximation and show that this results in a compressed pulse exhibiting pulse front tilt, whose magnitude is proportional to the normalized distance to the beam waist, providing a simple mechanism for controlling the tilt angle. We perform experimental measurements in a large-scale CPA laser for a range of beam curvatures that confirm these results.

1. Introduction

Over recent years, the development of ultrahigh intensity lasers capable of reaching the multi-petawatt regime has been impressive. Nowadays such systems are capable of providing pulses with energies of tens of Joules concentrated in durations of just a few optical cycles, in the femtosecond range. When focused, such pulses attain dramatic light intensities above 10^{22} W/cm^2, capable of driving electrons into the relativistic regime [1]. In order to generate such light pulses, these powerful devices make use of techniques such as chirped pulse amplification (CPA) [2] or optical parametric chirped pulse amplification (OPCPA) [3] consisting of pulse stretching and amplification followed by compression, which is almost ubiquitously performed using diffraction grating pairs.

Given the high energies involved and the limited damage threshold of the optical components used in laser systems, in particular diffraction gratings (<J/cm^2), it becomes necessary to magnify the laser beam as its energy grows. At the final compression stage, it is not unusual for a beam to have a diameter in the range of tens of cm. Such a large transverse dimension, combined with the narrow longitudinal extension associated to its ultrashort duration and the overall engineering complexity of the amplification chains make ultrahigh intensity pulses prone to a number of spatio-temporal couplings (STC) i.e. the pulse's spatial and temporal descriptions are not independent [4]. This usually leads to a number of undesired consequences, most importantly to a decrease of the focused peak intensity that can be very significant. On the other hand, the deliberate introduction and precise control of STC has allowed the optimization of several experimental setups in recent years, such as in controlling the velocity of ultrashort light pulses [5], isolated attosecond pulse generation [6], and ultrafast electron diffraction [7]. For these reasons, the full measurement of the spatio-temporal profile of high intensity pulses has also attracted a significant interest in recent years [8,9].

One of the most common STC is pulse-front tilt (PFT), a linear coupling between one spatial coordinate across the beam aperture and the arrival time of the intensity peak. A pulse exhibiting

#378935 https://doi.org/10.1364/OE.28.007678
Journal © 2020 Received 27 Sep 2019; revised 16 Nov 2019; accepted 18 Nov 2019; published 28 Feb 2020

Optics EXPRESS

PFT will have its pulse front at an angle relative to the wavefronts. In general, its electric field may be written as $E(x, t + \xi x)$, where ξ is the coupling parameter and the PFT angle is given by $\tan\gamma = c\xi$, with c the speed of light [10–12]. The interest of PFT is associated with its close interdependence with angular dispersion (AD), another STC characterized by a frequency-dependent propagation direction. In typical large-scale CPA/OPCPA schemes making use of angularly dispersive elements such as diffraction gratings and prisms, AD is an inherent feature that must be carefully taken into account. Essentially, an ultrashort pulse diffracted by a grating will acquire AD and PFT, and its duration will change with propagation distance. A second grating placed parallel to the first one at a specific distance will cancel these mechanisms, which is the principle underlying the grating pulse compressor. Normally, the compressor is double-passed (or a second similar compressor is employed) in order to remove a residual STC known as spatial chirp.

Grating compressors and their alignment issues have been studied in detail. Treacy [13] derived the expression for the quadratic frequency imparted by a grating pair in a plane wave approach, proposing its use as a pulse compressor. Martinez [14] derived the Gaussian beam transfer function for a single pass compressor and proposed the use of the double-pass compressor to eliminate spatial chirp. However, the analysis was limited to the case of a well-collimated input beam. Fiorini *et al.* [15] explored in detail the temporal pulse distortions resulting from misalignments in matched grating stretcher-compressor systems, using a Gaussian pulse formalism.

The generation and propagation of pulses exhibiting PFT and its relation with AD was explored by several authors [10,16,17] and the generation of PFT in CPA lasers was investigated both theoretically and experimentally [11,18,19]. These works were mostly focused on the temporal characteristics of the pulse, essentially assuming the good collimation condition and adopting the plane-wave approximation. The nature of PFT was further studied by Akturk *et al.* [12], who found a new mechanism, simultaneous temporal chirp and spatial chirp, capable of introducing PFT even in the absence of AD. Varjú *et al.* [20] analyzed the AD of ultrashort pulses taking into account a spatial Gaussian profile and verified that under certain parameters it can be substantially different from the case of a plane wave, however their analysis did not extend to the case of a grating compressor. The role of beam collimation in grating compressors was recently modelled using ray tracing sofware for the Vulcan high power laser, evidencing the appearance of STC in the focal plane, but without investigating their origin [21].

In this work we analyze the propagation of non-collimated laser pulses through a single-pass grating compressor and show that this effect leads to the creation of PFT in the compressed pulse, which does not happen when the good collimation approach is considered. We derive a simple relationship between the (normalized) distance to the beam waist and the PFT angle, showing that this method can be readily used as a source of tunable PFT in CPA lasers. The results are experimentally verified by changing the collimation of the compressor input beam in a high intensity laser system.

2. Theoretical model

2.1. Propagation of a general Gaussian beam through a grating compressor

In this section we will study the effect of a single pass compressor on a chirped pulse without the good collimation approximation. The compressor is designed to remove the existing chirp and normally the input beam is considered to be well collimated, leading to an approximate expression for the compressed pulse electric field. We assume that the compressor consists of two parallel diffraction gratings of groove density N and separated by a slant distance z. Fig. 1 shows the global geometry and the parameters used in the derivation. The input beam, at a wavelength λ, hits the first grating at an angle θ_i and is diffracted at an angle θ_d. The compressor

Optics EXPRESS

can be characterized by two parameters,

$$\alpha = \frac{\cos\theta_i}{\cos\theta_d} \qquad \beta = -\frac{N\lambda^2}{2\pi c\cos\theta_d} \tag{1}$$

where α is the grating anamorphic magnification and $\beta = d\theta_d/d\omega$ (fs) is the angular dispersion calculated at the central wavelength. We start from the analytical description introduced in [16], where the author derives the transfer function of the single pass grating compressor as (cf. Eq. 16 in that reference)

$$a(x,y,\omega) \propto \exp\left(i\frac{k\beta^2 z}{2}\omega^2\right)\exp\left\{-i\frac{k}{2}\left[\frac{(x+\alpha\beta z\omega)^2}{q\left(d+\alpha^2 z\right)}+\frac{y^2}{q(d+z)}\right]\right\} \tag{2}$$

where x is the dispersion plane and y is the plane perpendicular to it, ω and k are the frequency and wavenumber respectively, and $q(s) = s + iz_0$ is the Gaussian parameter for a beam of Rayleigh length z_0 whose waist is located a distance s away. In the case of the expression above, the length d, which will play an important role in the derivation, accounts for the distance between the beam waist plane and the compressor input, i.e. the first grating (see Fig. 1). Since for a general beam the Gaussian q-parameter is complex, it can be written as

$$\frac{1}{q\left(d+\alpha^2 z\right)} = \frac{1}{d+\alpha^2 z+iz_0} = \frac{d+\alpha^2 z-iz_0}{\left(d+\alpha^2 z\right)^2+z_0^2} \tag{3}$$

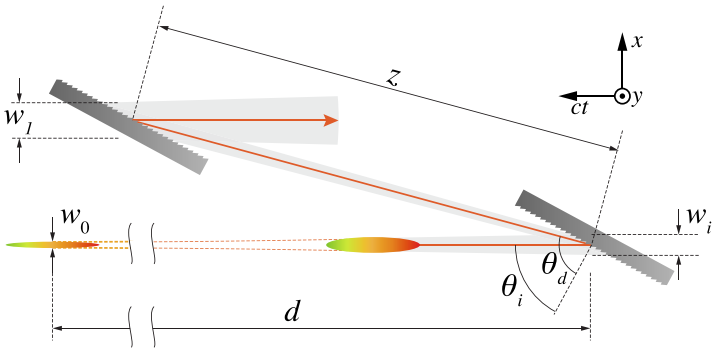

Fig. 1. Geometry for a single pass compressor assuming a non-collimated beam. The gratings are separated by a distance z, the incidence and diffracted angle are θ_i and θ_d respectively and the beam waist is located a distance d before the input plane. The beam waist is w_0 and the beam size before and after the compressor are w_i and w_1 respectively. The elements are not to scale and the beam divergence is exaggerated for illustration purposes.

A similar expression applies for the $y-$axis $q-$factor, with $\alpha = 1$ in that case. Because along this axis the beam propagation obeys a simple Gaussian evolution, in the following we ignore the $y-$dependence of the field. Separating the real and imaginary parts,

$$a(x,\omega) \propto \exp\left[-\frac{kz_0}{2}\frac{(x+\alpha\beta z\omega)^2}{z_x^2+z_0^2}\right]\exp\left(i\frac{k\beta^2 z}{2}\omega^2\right)\exp\left[-i\frac{kz_x}{2}\frac{(x+\alpha\beta z\omega)^2}{z_x^2+z_0^2}\right] \tag{4}$$

where we have introduced the overall propagation length $z_x = d + \alpha^2 z$ (the equivalent optical path length from the beam waist to the compressor output plane along the $x-$axis) to simplify the expressions. The good collimation condition corresponds to making $z_x/z_0 \approx 0$. In the Eq. above,

Optics EXPRESS

the real term represents the beam width together with a spectral filter that will broaden the pulse duration. The second term corresponds to the compressor group delay dispersion (GDD) and the third one, which does not appear in the good collimation approximation, can be considered a frequency-dependent beam divergence.

We now assume an input pulse of the form

$$E_i(\omega) = \exp\left(-\frac{\tau_0^2}{4}\omega^2\right)\exp\left(-i\frac{\varphi_{2p}}{2}\omega^2\right) \tag{5}$$

where τ_0 is the Fourier-transform limited pulse duration and φ_{2p} is the pulse GDD. An ideal compressor will cancel the dispersion i.e. the phase terms in ω^2. For the well-collimated beam approximation this happens for the grating separation $z = \varphi_{2p}/k\beta^2$. We assume that the compressor has been adjusted to this configuration, so that the output pulse is given by

$$\begin{aligned} E(x,\omega) = E_i(\omega)a(x,\omega) &= \exp\left(-\frac{\tau_0^2\omega^2}{4}\right)\exp\left[-\frac{kz_0}{2}\frac{(x+\alpha\beta z\omega)^2}{z_x^2+z_0^2}\right]\exp\left[-i\frac{kz_x}{2}\frac{(x+\alpha\beta z\omega)^2}{z_x^2+z_0^2}\right] \\ &= \exp\left(-\frac{\tau_0^2\omega^2}{4}\right)\exp\left[-\frac{1}{w_i^2}(x-\zeta\omega)^2\right]\exp\left[-i\frac{\rho}{w_i^2}(x-\zeta\omega)^2\right] \end{aligned} \tag{6}$$

where the spatial chirp term is given by $\zeta = -\alpha\beta z$ and we have introduced the normalized optical path length $\rho = z_x/z_0$. For a beam waist w_0, the term $w_i = w_0\sqrt{1+(z_x/z_0)^2} = w_0\sqrt{1+\rho^2}$ represents the beam width at the plane equivalent to the compressor output. However, even for slightly uncollimated beams the compressor length will be much smaller than the distance to the waist, i.e. $z \ll d$, such that the beam width change during propagation through the compressor may be neglected. For that reason, we may label w_i as the *input* beam width at the compressor (Fig. 1) and the Gaussian beam behavior is preserved in the phase term.

We now adopt an approach similar to that followed in [12] and rearrange the real part of Eq. (6) to obtain

$$E(x,\omega) = E_0\exp\left(-\frac{x^2}{w_1^2}\right)\exp\left[-\frac{\tau_1^2}{4}(\omega-\nu x)^2\right]\exp\left[-i\frac{\rho}{w_i^2}(x-\zeta\omega)^2\right] \tag{7}$$

where

$$\nu = \frac{\zeta}{\frac{w_i^2\tau_0^2}{4}+\zeta^2} \qquad \tau_1 = \left(\tau_0^2+\frac{4\zeta^2}{w_i^2}\right)^{1/2} \qquad w_1 = \left(\frac{1}{w_i^2}-\frac{\tau_1^2\nu^2}{4}\right)^{-1/2} \tag{8}$$

are the frequency gradient ($d\omega/dx$), the local pulse width (larger than τ_0 due to the decreased available bandwidth caused by the spatial chirp) and the beam width (larger than the input width due to the transverse frequency spread). Equation (7) is useful in order to visualize the structure of the inhomogeneous pulse. The first two terms describe the pulse intensity in the space and frequency domains. At any position x, the bandwidth is constant and given by $\tau_1/2$, so the local pulse duration is the same across the beam aperture. The local central frequency at each slice is given by the frequency gradient, $\omega_0(x) = \nu x$, so the second exponential represents the spatial chirp. The last exponential, which is specific of non-collimated beams, represents a coupling between x and ω that accounts for the beam radius of curvature and that will result in pulse front tilt. This identification is described in Appendix 1, here we continue with a more formal derivation with the goal of obtaining the electric field in the time domain.

Optics EXPRESS

It is convenient at this stage to use the parameter u originally introduced in [16] to qualify a good compressor design,

$$u = \left(\frac{2\alpha\beta z}{w_i\tau_0}\right)^2 = \frac{4\zeta^2}{w_i^2\tau_0^2} \tag{9}$$

By using this definition, Eqs. (8) may be rewritten compactly as

$$\nu = \frac{1}{\zeta}\frac{u}{u+1} \qquad \tau_1 = \tau_0\sqrt{1+u} \qquad w_1 = w_i\sqrt{1+u} \tag{10}$$

For a good compression, the condition $u \approx 0$ should be attained.

We now consider the imaginary part of Eq. (7) and rearrange it in a similar way in order to introduce the dependence $\omega - \nu x$. After several steps, we obtain

$$\begin{aligned} E(x,\omega) = E_0 \exp\left(-\frac{x^2}{w_1^2}\right)\exp\left(-i\rho\frac{x^2}{w_1^2}\right) \\ \times \exp\left[-\frac{\tau_1^2}{4}(\omega-\nu x)^2\right]\exp\left[-i\frac{\rho\zeta^2}{w_i^2}(\omega-\nu x)^2\right] \\ \times \exp\left[i\frac{2\rho\zeta^2}{w_i^2}\left(\frac{1}{\zeta}-\nu\right)x(\omega-\nu x)\right] \end{aligned} \tag{11}$$

This expression is similar to that of Eq. (10) in [12], which represents a Gaussian pulse with GDD and AD. By comparing the last two exponentials, the following identifications can be made for the respective coefficients:

$$\varphi_2 = \frac{2\rho\zeta^2}{w_i^2} \qquad k_0\beta = -\frac{2\rho\zeta}{w_i^2} \tag{12}$$

This means that a non-collimated beam will emerge from a single pass compressor with residual AD and GDD, proportional to the normalized waist distance ρ, and consequently the beam will also exhibit PFT. This is a new result when compared to the collimated beam approximation.

In order to obtain the pulse in the time domain, we perform an inverse Fourier transform, resulting in

$$\begin{aligned} E_0(x,t) \propto E_0 \exp\left(-\frac{x^2}{w_1^2}\right)\exp\left[\mathrm{i}\frac{(2u-1)\rho}{w_1^2}x^2\right]\exp\left[-\frac{(t-\xi x)^2}{\tau^2}\right] \\ \times \exp\left\{\mathrm{i}\left[\phi_1\,(t-\xi x) + \frac{\phi_2}{2}\,(t-\xi x)^2\right]\right\} \end{aligned} \tag{13}$$

with the following definitions:

$$\phi_1 = \frac{1}{\zeta}\frac{ux}{u+1} \qquad \phi_2 = \frac{1}{\tau_0^2}\frac{2u\rho}{(1+u)^2+u^2\rho^2} \tag{14}$$

$$\tau = \left[\tau_1^2 + \left(\frac{2\varphi_2}{\tau_1}\right)^2\right]^{1/2} = \tau_1\left[1+\left(\frac{\rho u}{1+u}\right)^2\right]^{1/2} = \tau_0\left[(1+u)+\frac{u^2}{1+u}\rho^2\right]^{1/2} \tag{15}$$

Using the definition of [12], the pulse front tilt is given by

$$\xi = k_0\beta + \varphi_2\nu = \frac{2\rho\zeta}{w_i^2}(-1+\zeta\nu) = -\frac{2\rho\zeta}{w_i^2}\frac{1}{1+u} \tag{16}$$

where the first of Eqs. (10) was used. Assuming that the good compressor design criterion is met ($u \approx 0$), we have $k_0\beta \gg \phi_2\nu$, from which we may conclude that the PFT is mostly originated

Optics EXPRESS

from AD, with only a small fraction (ratio $u/(u+1)$) originating from spatial and temporal chirp. By using the definitions of ζ and u the PFT may also be written in terms of the input pulse and normalized parameters as

$$\xi = -\frac{2\alpha\beta z}{w_i^2}\frac{\rho}{1+u} = \frac{\tau_0}{w_i}\frac{\rho\sqrt{u}}{1+u} \tag{17}$$

We can see that by adjusting the normalized distance $\rho \approx d/z_0$ between beam waist and compressor input (i.e. the beam divergence) it becomes possible to introduce a controllable PFT in the output pulse. The pulse also exhibits a residual GDD (chirp parameter ϕ_2) due to the beam divergence, compared to the well-collimated case. In the limit $\rho \ll 1$, Eq. (13) becomes simply

$$E_0(x,t) \propto \exp\left(-\frac{1}{1+u}\frac{x^2}{w_i^2}\right)\exp\left(-\frac{1}{1+u}\frac{t^2}{\tau_0^2}\right)\exp\left(-\frac{iuxt}{(1+u)\alpha\beta z}\right) \tag{18}$$

which is the compressed output pulse in the good collimation condition [14], without residual GDD or PFT. Figure 2 illustrates the main differences between the two cases, with the well-collimated beam (top) and non-collimated beam (bottom) situations. For a diverging beam (ρ>0), as shown, the beam is tilted such that the high frequencies arrive first and the pulse exhibits a residual positive chirp for each x-position; the opposite happens for a converging beam (ρ<0).

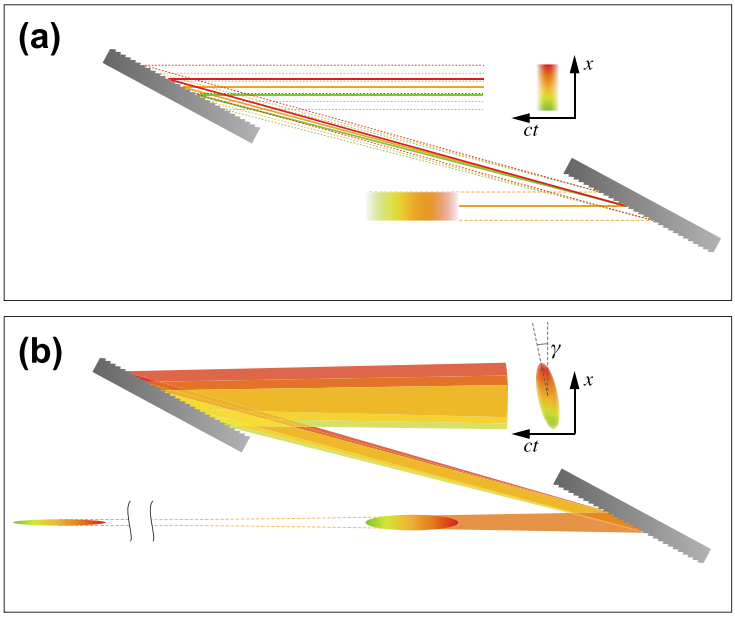

Fig. 2. Top: well-collimated beam propagating through a single-pass pulse compressor, showing simple spatial chirp at the exit. Bottom: diverging Gaussian beam propagating through the same compressor, with the beam waist illustrated on the bottom left. The output pulse exhibits pulse front tilt and a residual GDD. The elements are not to scale and the beam divergence is exaggerated for illustration purposes.

In the case of a double pass compressor, the scenario is significantly different. For that situation, the starting transfer function is given by Eq. (44) in [16],

$$a(x,y,\omega) \propto \exp\left(ik\beta^2\omega^2 z\right)\exp\left\{-i\frac{k}{2}\left[\frac{x^2}{q\,(d+2\alpha^2 z)} + \frac{y^2}{q(d+z)}\right]\right\} \tag{19}$$

Optics EXPRESS

where the distance between passes and post-compressor propagation were ommitted for simplicity. It is clear that even in the non-collimated beam approach the compressor can be designed to remove the chirp exactly and that no STC will result. This contrasts with the use of a misaligned double-pass compressor to generate PFT [11,18,19], where the second pass effectively doubles the tilt angle.

2.2. Limitations for ultrashort pulses

In a first approach, the model derived in the previous section does not make any approximation that limits its validity for the case of ultrashort pulses in the femtosecond range. However there are practical limitations to its application, which we discuss here. Given their large bandwidth, femtosecond systems typically employ double pass compressors (for which the condition $u \approx 0$ is not required), because the residual spatial chirp introduced in a single pass would not be acceptable and because of the moderate grating size and space requirements. In contrast, single pass compressors are often a good compromise for high energy, picosecond-level pulses, for which a double pass would require more space, larger or additional gratings and a significant energy loss.

We can nevertheless consider the case of a well-designed single pass compressor for femtosecond pulses by requiring the condition $u \approx 0$. For example, let us compare a 10 cm diameter, 1 ps pulse and a 1 cm diameter, 10 fs pulse. The product $w_i\tau_0$ for the second case is 1000 times smaller than for the first, so a comparable value for u would require that the spatial chirp coefficient ζ is smaller by the same ratio (cf. Eq. (9)). However, the resulting PFT would be 10 times smaller for the same value of ρ (cf. Eq. (16)). In order to obtain the same PFT as for the picosecond-scale compressor, the femtosecond-scale beam would have to be enlarged to 10 cm. While this would also decrease the frequency gradient ν and the associated spatial chirp, it would be unpractical from a laser system engineering point of view. Therefore, from a practical viewpoint the model proposed here is mostly targeted at high energy laser systems that already make use of a single pass compressor.

3. Measuring pulse front tilt from non-collimated beams

3.1. Experimental setup and introduction of beam divergence

In order to test experimentally the validity of the results from the previous section, we fitted a CPA laser system with an adjustable imaging telescope allowing us to control the compressor input beam divergence. Figure 3 shows a schematic of the main components of the laser system and the diagnostics used. The beam coming from the stretcher has a width w_s and propagates through an image relay system composed of four lens pairs arranged in consecutive spatial filter setups, such that the second lens of pair n images the beam onto the first lens of pair $n+1$. The first spatial filter (lenses f_1, f_2) is equipped with a translation stage that allows adjusting the separation between its lenses by a variable amount Δf. The last spatial filter images the beam onto the compressor input plane. This imaging system, which will define the values of d and z_0 at the compressor input, may be represented by the $ABCD$ matrix

$$\begin{pmatrix} M\left(1-\frac{\Delta f}{f_1}\right) & M\Delta f \\ -\frac{\Delta f}{Mf_1^2} & \frac{1}{M}\left(1+\frac{\Delta f}{f_1}\right) \end{pmatrix} \tag{20}$$

where M is the overall magnification of the imaging system, f_1 is the focal length of the first lens and Δf is the displacement of this lens with respect to the correct distance $(f_1 + f_2)$ to the second lens. Assuming that the input beam meets lens f_1 at the waist plane:

- for $\Delta f = 0$ this represents a simple imaging system such that the compressor input beam will also be at the waist plane;

Optics EXPRESS

- for $\Delta f \neq 0$ and assuming $\Delta f/f_1 \ll 1$, by applying the propagation rule for the Gaussian $q-$parameter we find for the compressor input beam

$$z_0 = \frac{M^2 z_{0s}}{1+\left(\frac{z_{0s}\Delta f}{f_1^2}\right)^2} \qquad d = -\frac{M^2 \Delta f (z_{0s}/f_1)^2}{1+\left(\frac{z_{0s}\Delta f}{f_1^2}\right)^2} = -\frac{z_{0s} z_0}{f_1^2}\Delta f \tag{21}$$

where $z_{0s} = \pi w_{0s}^2/\lambda$ is the Rayleigh length of the stretcher beam.

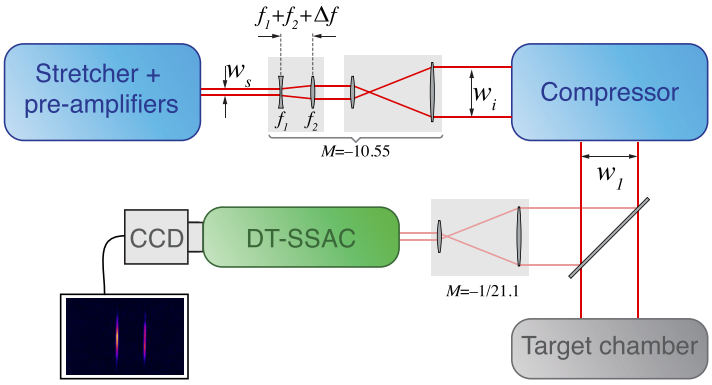

Fig. 3. Experimental setup for PFT characterization. Chirped pulses from the stretcher are magnified and imaged onto the single pass grating compressor. The output pulses are demagnified and sent to a double-trace single shot autocorrelator (DT-SSAC) diagnostic.

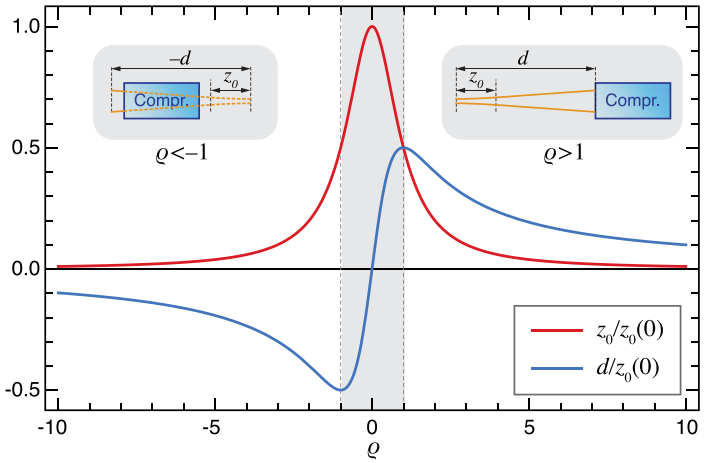

Fig. 4. Rayleigh length z_0 (red) and distance to beam waist d (blue) normalized to the well-collimated beam Rayleigh length vs. length parameter ρ.

Therefore, the normalized length parameter may be written as

$$\rho \approx \frac{d}{z_0} = -\frac{z_{0s}}{f_1^2}\Delta f \tag{22}$$

We can also express Eqs. (21) in terms of this parameter,

$$z_0 = \frac{M^2 z_{0s}}{1+\rho^2} \qquad d = -\frac{M^2 z_{0s}\rho}{1+\rho^2} = \rho z_0 \tag{23}$$

Optics EXPRESS

Fig. 4 shows the variation of z_0 and d, normalized to the well-collimated ($\Delta f = 0$) case, over a range of values of ρ. The insets illustrate the beam collimation conditions for different regions, as described below:

- $\rho = 0$ corresponds to the the well-collimated case ($d = 0$).
- ρ>1: the beam is diverging (d>z_0). As ρ increases, d decreases, corresponding to a smaller Gaussian radius of curvature, i.e. stronger divergence.
- ρ< − 1: the beam is converging, with the waist plane located beyond the compressor ($-d$>z_0). As ρ decreases, $|d|$ decreases, corresponding to stronger convergence.
- −1<ρ<1 (grey region): the compressor is located within the Rayleigh range ($|d|$<z_0). Because the radius of curvature of a Gaussian beam varies strongly within this region, this type of configuration is not desirable for the goal of generating a controllable PFT, due to a larger chance of experimental errors.

By making use of Eq. (23) and of $w_0^2 = \lambda z_0/\pi$, we may write for the beam radius at the compressor input plane,

$$w_i = w_0\sqrt{1 + (d/z_0)^2} \approx \sqrt{\frac{\lambda}{\pi} z_0 \left(1 + \rho^2\right)} = M\sqrt{\frac{\lambda z_{0s}}{\pi}} \tag{24}$$

Finally, putting together Eqs. (22) and (24) and replacing in Eq. (16),

$$\tan\gamma = -\frac{2\alpha\beta c z}{w_i^2}\frac{\rho}{1+u} = -\frac{\omega_0 \zeta \Delta f}{M^2 f_1^2 (1+u)} \tag{25}$$

where $\omega_0 = 2\pi c/\lambda$ is the central pulse frequency. This simple expression only depends on the pulse parameters through the u coefficient and indicates that the PFT varies linearly with the defocusing distance Δf. Additionally, assuming that the compressor has been well designed to meet $u \approx 0$ for the input beam width and pulse duration, the last expression shows that the residual PFT is essentially proportional to $\zeta = -\alpha\beta z$ and consequently to the grating separation and angular dispersion. This becomes especially relevant for high intensity laser systems, where the wide beam diameters and high intensities involved require long compressor distances and large stretching-compression factors.

3.2. Experimental parameters and methods

The measurements were performed using the Vulcan Nd:glass CPA laser system as a source and the Target Area West single pass pulse compressor. The compressor and beam parameters are shown in detail in Table 1. When collimated, the compressor input beam has an equivalent beam diameter of 185 mm, although an apodizer limits the actual beam aperture to the grating size. This wide beam size, coupled with a subpicosecond pulse duration, result in an almost negligible value for the u parameter. The grating separation was first adjusted to provide the minimum pulse duration for the $\Delta f = 0$ configuration. For the measurements, the first lens (f_1 =0.6 m) position was scanned in steps of 2 mm from $\Delta f = -8$ mm ($\rho = 32.8$) to +4 mm ($\rho = -16.4$), well within the approximation $\Delta f \ll f_1$. A number of acquisitions was made for each position. The beam emerging from the compressor was demagnified using a series of imaging lenses with a total magnification of 1/21.1 and sent to the diagnostics table.

To characterize the pulse we used a double trace autocorrelator, whose setup and operation are described in detail in [22]. Essentially, this device is capable of providing independent and simultaneous readings of the pulse duration and PFT, and in our implementation it was optimized for measuring pulses within the expected range of the compressed pulse duration. It works by crossing a single pulse with two consecutive replicas inside a nonlinear crystal, such that

Optics EXPRESS

Table 1. List of the experimental parameters used.

Parameter	Symbol	Value	Units
Input pulse			
Central wavelength	λ_0	1053.5	nm
TL pulse duration	τ_0	800	fs
Stretcher beam diameter	w_{0s}	0.0175	m
Stretcher beam Rayleigh length	z_{0s}	913	m
Compressor			
Grating separation	z	3.5	m
Grating groove density	N	1740	mm^{-1}
Incident angle	θ_i	61.00	°
Diffracted angle for λ_0	θ_d	73.43	°
Anamorphic magnification	α	1.7	
Grating dispersion	β	−3.59	fs
Coupling parameters			
Compressor factor	u	0.084	
Spatial chirp	ζ	21.37	m.fs
Frequency gradient	ν	3.6×10^{-3}	$\mathrm{m}^{-1}\mathrm{fs}^{-1}$

two parallel autocorrelation traces are obtained. The pulse duration can be obtained from the autocorrelation trace as usual, and the PFT value and sign are obtained from changes to the separation between the two traces.

4. Results and discussion

Figure 5 shows the measured PFT (top) and pulse duration (bottom) for different amounts of defocusing. Concerning the PFT, by applying the parameters of Table 1 to Eq. (25) and considering the beam demagnification factor, we obtain the linear relationship $\gamma[\mathrm{mrad}] \approx 18.6 \times \Delta f[\mathrm{mm}]$, plotted as the straight red line in the top figure. For the tested beam parameters, the overlap is excellent, with the fluctuations being due to a slight inhomogeneous beam shape from one shot to the next. The low value of u means that the measured PFT derives almost exclusively from the residual AD. With this method, and for a lens shift of only $\Delta f = 8$ mm, a maximum PFT angle of 148 mrad in a ≈ 1 cm diameter beam was obtained. It should be stressed that at the focal spot this value would be much larger, making the PFT generated by this method far from residual. From Eq. (25) we can see that this method of generating a controllable PFT is highly versatile, allowing different degrees of freedom independent from the compressor design (e.g. focal lens f_1, magnification M between the first lens and the input grating, amount of defocusing Δf). This contrasts with the traditional method of slightly misaligning the second grating in a double-passed grating compressor, where the misalignment angle is the only parameter independent from the compressor design. Besides, the latter method requires also misaligning the return mirror in order to recover the output beam alignment, making it particularly unsuitable for large aperture setups involving multiple tiled gratings. In contrast, our method preserves the full alignment through the compressor at all times, allowing continuous monitoring of the pulse parameters.

The pulse duration was measured simultaneously with the double trace autocorrelator and with a traditional single-shot autocorrelator, yielding identical results. The parabolic red line in Fig. 5 (bottom) represents the expression of Eq. (15) for the pulse duration, which links the increased pulse duration to the residual GDD associated to a non-collimated beam. The experimental points

Optics EXPRESS

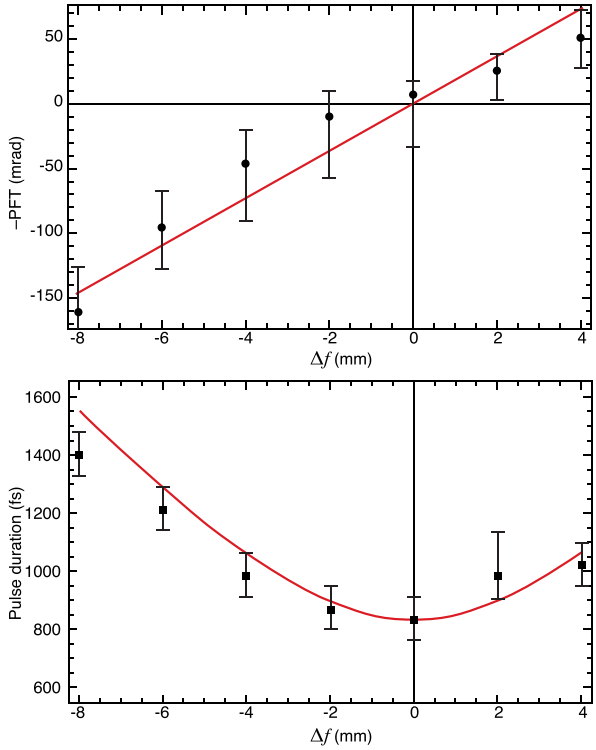

Fig. 5. Experimental measurements for the pulse front tilt angle (top) and pulse duration (bottom) as a function of the telescope lens displacement.

have a good agreement in this case, with small differences (<10%) for the longer pulse durations. This may be linked to the u^2 dependence of the curvature and the experimental uncertainty in the determination of a rigorous value for u, in particular the exact determination of the spatial parameters of the stretcher output beam.

5. Conclusions

We have analyzed the propagation of Gaussian beams through a grating compressor without applying the usual well-collimated beam approximation. We used the transfer function of the single-pass grating compressor, including the beam divergence term, and showed that the output beam will exhibit spatio-temporal couplings, which do not appear when the above approximation is used. In particular, the emergence of PFT with magnitude proportional to the normalized distance to the beam waist is a major consequence of this approach. We derived a simple expression relating the PFT coupling parameter ξ with the pulse and compressor properties and discussed the mechanisms underlying its generation.

We designed an experiment to test this result by using an adjustable telescope in the beam magnification system before the compressor in a CPA laser. We derived the expression linking the expected PFT and found that for small deviations it is proportional to the telescope lens shift. This also lead to a simple expression for the resulting PFT angle. We performed experimental measurements for both diverging and converging beams and obtained results that validate the calculated expressions. This shows that this mechanism can be used as a source of tunable PFT in CPA lasers without the need to misalign the grating compressor. On the other hand, our results also allow estimating the sensitivity of a CPA compressor to the beam collimation when no STC

Optics EXPRESS

are desired. These results are useful both for the design of ultrahigh intensity laser systems and for laser experiments using geometries based on tilted pulse front excitation.

Appendix: Alternative derivation of the expression for the pulse front tilt

It is possible to derive the expression for the overall pulse front tilt (Eq. (16)) in a more straightforward fashion by using the general theory of STC [12]. Let us consider the phase of the electric field in Eq. (7),

$$\frac{\rho}{w_i^2}(x-\zeta\omega)^2 \tag{26}$$

Just as the real part of Eq. (7) represents an intensity coupling between x and ω, associating a central frequency to each position across the beam aperture (i.e. spatial chirp), the expression above represents a phase coupling, associating a temporal chirp to the spherical beam wavefront at a given position. For each position x, there is a central frequency $\omega_0(x) = x/\zeta$ for which this chirp is cancelled, so that for different propagation directions across the Gaussian beam aperture there will be a constant chirp but a linearly varying central frequency. Expanding now the Eq. above,

$$\frac{\rho}{w_i^2}(x^2 - 2\zeta\omega + \zeta^2\omega^2) = R^I_{xx}x^2 + 2R^I_{x\omega}x\omega - R^I_{\omega\omega}\omega^2 \tag{27}$$

where the different R are the imaginary parts of the spatio-temporal coupling coefficients in the (x, ω) domain, we may make the following identifications:

- R^I_{xx} represents the beam radius of curvature, associated to its divergence
- $R^I_{x\omega} = \rho\zeta/w_i^2$ is associated to a STC named wavefront tilt dispersion (WFD)
- $R^I_{\omega\omega} = \rho\zeta^2/w_i^2$ is the linear frequency chirp (FCH) coefficient

Because the STC in different domains are related by means of Fourier transforms, it is possible to express pulse front tilt, which is a coupling in the (x, t) domain, in terms of the above couplings, resulting in Eq. (48) in [12])

$$\mathrm{PFT} = -2 \times \mathrm{WFD} + 2\mathrm{FCH} \times \mathrm{FRG} \tag{28}$$

where FRG stands for frequency gradient i.e. ν. Replacing by the corresponding expressions, we obtain

$$\xi = -\frac{2\rho\zeta}{w_i^2} + \frac{2\rho\zeta^2}{w_i^2}\nu \tag{29}$$

which is equivalent to Eq. (16).

Funding

Horizon 2020 Framework Programme (GA654148); Fundação para a Ciência e a Tecnologia (ROTEIRO/0075/2013); Fundação para a Ciência e a Tecnologia (SFRH/BSAB/135557/2018, PD/BD/114327/2016).

Disclosures

The authors declare that there are no conflicts of interest related to this article.

Optics EXPRESS

References

1. G. A. Mourou, T. Tajima, and S. V. Bulanov, "Optics in the relativistic regime," Rev. Mod. Phys. **78**(2), 309–371 (2006).
2. P. Maine, D. Strickland, P. Bado, M. Pessot, and G. Mourou, "Generation of ultrahigh peak power pulses by chirped pulse amplification," IEEE J. Quantum Electron. **24**(2), 398–403 (1988).
3. I. Ross, P. Matousek, M. Towrie, A. J. Langley, and J. L. Collier, "The prospects for ultrashort pulse duration and ultrahigh intensity using optical parametric chirped pulse amplifiers," Opt. Commun. **144**(1-3), 125–133 (1997).
4. S. Akturk, X. Gu, P. Bowlan, and R. Trebino, "Spatio-temporal couplings in ultrashort laser pulses," J. Opt. **12**(9), 093001 (2010).
5. A. Sainte-Marie, O. Gobert, and F. Quéré, "Controlling the velocity of ultrashort light pulses in vacuum through spatio-temporal couplings," Optica **4**(10), 1298–1304 (2017).
6. H. Vincenti and F. Quéré, "Attosecond lighthouses: how to use spatiotemporally coupled light fields to generate isolated attosecond pulses," Phys. Rev. Lett. **108**(11), 113904 (2012).
7. P. Zhang, J. Yang, and M. Centurion, "Tilted femtosecond pulses for velocity matching in gas-phase ultrafast electron diffraction," New J. Phys. **16**(8), 083008 (2014).
8. C. Dorrer, "Spatiotemporal metrology of broadband optical pulses," IEEE J. Sel. Top. Quantum Electron. **25**(4), 1–16 (2019).
9. G. Pariente, V. Gallet, A. Borot, O. Gobert, and F. Quéré, "Space-time characterization of ultra-intense femtosecond laser beams," Nat. Photonics **10**(8), 547–553 (2016).
10. Z. Bor, B. Rácz, G. Szabó, M. Hilbert, and H. A. Hazim, "Femtosecond pulse front tilt caused by angular-dispersion," Opt. Eng. **32**(10), 2501–2504 (1993).
11. G. Pretzler, A. Kasper, and K. Witte, "Angular chirp and tilted light pulses in CPA lasers," Appl. Phys. B: Lasers Opt. **70**(1), 1–9 (2000).
12. S. Akturk, X. Gu, E. Zeek, and R. Trebino, "Pulse-front tilt caused by spatial and temporal chirp," Opt. Express **12**(19), 4399–4410 (2004).
13. E. Treacy, "Optical pulse compression with diffraction gratings," IEEE J. Quantum Electron. **5**(9), 454–458 (1969).
14. O. E. Martinez, "Grating and prism compressors in the case of finite beam size," J. Opt. Soc. Am. B **3**(7), 929–934 (1986).
15. C. Fiorini, C. Sauteret, C. Rouyer, N. Blanchot, S. Seznec, and A. Migus, "Temporal aberrations due to misalignments of a stretcher-compressor system and compensation," IEEE J. Quantum Electron. **30**(7), 1662–1670 (1994).
16. O. E. Martinez, "Pulse distortions in tilted pulse schemes for ultrashort pulses," Opt. Commun. **59**(3), 229–232 (1986).
17. J. Hebling, "Derivation of the pulse front tilt caused by angular dispersion," Opt. Quantum Electron. **28**(12), 1759–1763 (1996).
18. J.-C. Chanteloup, E. Salmon, C. Sauteret, A. Migus, P. Zeitoun, A. Klisnick, A. Carillon, S. Hubert, D. Ros, P. Nickles, and M. Kalachnikov, "Pulse-front control of 15-TW pulses with a tilted compressor, and application to the subpicosecond traveling-wave pumping of a soft-x-ray laser," J. Opt. Soc. Am. B **17**(1), 151–157 (2000).
19. K. Osvay, A. P. Kovács, Z. Heiner, G. Kurdi, J. Klebniczki, and M. Csatari, "Angular dispersion and temporal change of femtosecond pulses from misaligned pulse compressors," IEEE J. Sel. Top. Quantum Electron. **10**(1), 213–220 (2004).
20. K. Varjú, A. P. Kovács, K. Osvay, and G. Kurdi, "Angular dispersion of femtosecond pulses in a Gaussian beam," Opt. Lett. **27**(22), 2034–2036 (2002).
21. R. Heathcote, M. Galimberti, R. J. Clarke, T. B. Winstone, I. O. Musgrave, and C. Hernandez-Gomez, "Collimation effects on large CPA compressors," Appl. Phys. B: Lasers Opt. **116**(4), 805–809 (2014).
22. G. Figueira, L. Braga, S. Ahmed, A. Boyle, M. Galimberti, M. Galletti, and P. Oliveira, "Simultaneous measurement of pulse front tilt and pulse duration with a double trace autocorrelator," J. Opt. Soc. Am. B **36**(2), 366–373 (2019).